J. Membrane Biol. 138, 77–89 (1994)

The Journal of
Membrane
Biology
© Springer-Verlag New York Inc. 1994

Open States of Nuclear Envelope Ion Channels in Cardiac Myocytes

J.O. Bustamante
Departments of Medicine and Physiology, Division of Cardiology—Heart Center, University of Maryland School of Medicine, 655 West Baltimore, Baltimore, Maryland 21201-1559

Received: 16 July 1993/Revised: 18 October 1993

Abstract. Prevalent nucleocytoplasmic transport theory views flow of monoatomic ions as completely unrestricted, resulting from the presence of large diameter pore complexes (NPCs) that perforate, but hold together, the two separate membranes of the nuclear envelope (NE). However, three lines of investigations indicate that, at least in some cell types, monoatomic ion flow is restricted. (i) Patch clamp reveals quantized, ion channel-like activity in several NE preparations; activity thought to result from nuclear ion channels (NICs) connected to NPCs. (ii) Ratiometric fluorescence microscopy demonstrates that ions, as well as small molecules relevant to signal transduction, do distribute as if there is a NE barrier. (iii) Electron microscopy shows that NPCs contain material that behaves like a plug. NICs' large conductance (up to 1,000 pS) makes them a major determinant of nuclear ion concentrations which, in turn, influence nuclear processes. Therefore, NICs are an important modulating force of gene and transcriptional activities—two major determinants of gene expression. As nuclear processes may take from seconds (e.g., signaling) to minutes (e.g., transcription), the time the channels dwell in the ion-conducting open state is relevant to understanding NICs' role in nuclear function. Consequently, dwell-times and lifetimes of open NIC states were studied in 61 patch-clamped adult mouse cardiac myocyte nuclei. Upon voltage stimulation, NICs opened to main states of large conductance (281 ± 198 pS, range = 120–490 pS, n = 55) and wide-range mean dwell-times (~100 msec, 1–10 sec, and min). Closed states (0 pS) also had widely distributed mean dwell-times (~100 msec, 1–10 sec, and min). Putative open substates (37 ± 11 pS, range = 25–50, pS, n = 6) of high bursting frequency (<1 msec) were observed without intervening main states (≈5% of patches). Fast (~0.1 msec) and slow (~10 msec) state-transitions were also detected. These observations suggest a role for NICs in mediating cytoplasmic signal control of cardiomyocyte gene expression.

Key words: Cardiac — Nucleus — Nuclear envelope — Nuclear pore complex — Nuclear ion channels — Channel conductance

Introduction

Nuclear envelope ion channels have been recently identified in animal and plant cells (Matzke, Weiger & Matzke, 1990; Mazzanti et al., 1990; Mazzanti, DeFelice & Smith, 1991; Tabares, Mazzanti & Clapham, 1991; Bustamante, 1992, 1993; Matzke et al., 1992; Innocenti & Mazzanti, 1993; *reviewed in* Bustamante, 1994) and support classical observations of high envelope resistance to ion flow (e.g., Loewenstein & Kanno, 1962; *see* Bustamante, 1994). Electron microscopy suggests that nuclear ion channels (NICs) may derive from nuclear pore complexes (NPCs) because envelope patches displaying ion channel activity contain pore complexes (e.g., Mazzanti et al., 1991; Matzke et al., 1992). Electron microscopy also demonstrates that NIC activity is intrinsic to the envelope because ion channel currents are recorded in preparations lacking endoplasmic reticulum and Golgi apparatus (Matzke et al., 1990, 1992). Ratiometric fluorescence microscopy shows unequal distribution of ions and small molecules between the nucleus and cytoplasm (e.g., Williams et al., 1985; Hernández-Cruz, Sala & Adams, 1990; Neylon et al., 1990; Takamatsu & Wier, 1990; Hernández-Cruz, Sala & Connor, 1991; Przywara et al., 1991; Waybill et al., 1991) and also shows electrical potential gradients across the envelope (e.g., Matzke & Matzke, 1986; Matzke, Matzke & Neuhaus, 1988; *see review by* Matzke & Matzke, 1991). This chemical and electrical

heterogeneity has been interpreted in terms of a resistive nuclear envelope (NE; e.g., Hernández et al., 1991; *see also* Bustamante, 1994). Work with high-resolution electron microscopy reveals that nuclear pores are not permanently opened but that they are gated by a large plug (~MD; e.g., Akey, 1989, 1990, 1991, 1992; Akey & Goldfarb, 1989; Dingwall, 1990, 1991; Reichelt et al., 1990; Jarnik & Aebi, 1991; Akey & Radermacher, 1993). Eight small channels peripheral and parallel to the large NPC central channel have been proposed to underly transport of inorganic ions and other small solutes (Hinshaw, Carragher & Milligan, 1992). However, this observation could not be confirmed (Akey & Radermacher, 1993).

The potential relevance of nuclear envelope ion channels to nuclear function is stressed by these ion channels having a high gated conductance—which may reach up to 1,000 pS. Nuclear ion concentration change resulting from NIC activity is far from negligible and, thus, it might impact on nuclear processes such as gene activity and transcription (*see* Bustamante, 1994). Therefore, since the characteristic times of nuclear processes cover a wide range of values (frequently taking many minutes), it is important to determine whether nuclear envelope ion channels dwell in the open states for periods of time that can be related to these processes.

The patch-clamp study presented here addressed this subject by focusing on the open, conducting dwell-times for NICs from adult mouse cardiac myocytes (Bustamante, 1992, 1993). These differentiated, committed muscle cells have been the subject of investigation by this investigator for over a decade (e.g., Bustamante, Watanabe & McDonald, 1981, 1982; Bustamante et al., 1982; Bustamante & McDonald, 1983). Therefore, techniques for the preparation of these myocytes ensure the normal structure and function of the preparation. As one of the interests of this author is to understand the mechanisms underlying development of cardiac hypertrophy (e.g., Bustamante, Ruknudin & Sachs, 1991; Ruknudin, Saks & Bustamante, 1993) and the expression and metabolism of cardiac peptides (Boer et al., 1991), the study of adult cardiac myocyte NICs was deemed a pivotal experimental approach to this task (Bustamante, 1992).

The results confirmed the quantized, discrete nature of cardiac myocyte NIC open states (Bustamante, 1992, 1993), resembling that of (double-membrane) gap junctional channels (e.g., Loewenstein, Kanno & Socolar, 1978; Loewenstein, 1981; Neyton & Trautmann, 1985; Burt & Spray, 1988; Veenstra, 1990; Manivannan et al., 1992). The studies also showed that NIC dwell-times cover a wide range of values, suggesting a large interaction with and/or potential role in nuclear processes. As NIC activity (recorded as ion currents) may reflect the magnitude of nucleocytoplasmic exchange of ribonucleoproteins, etc., the experimental results described here may help understand transduction signal control of gene activity, in particular, and of nuclear processes, in general (e.g., Karin, 1991; Baeuerle & Lührmann, 1991; Davis, 1992; Hanover, 1992). Consequently, these investigations may serve to establish a guideline to link surface membrane signaling (e.g., stretch, *see* Bustamante et al., 1991; Ruknudin et al., 1993) to activation of myocyte growth and hypertrophy and with cardiac peptide processing and secretion following mechanical load (e.g., Boer et al., 1992).

Materials and Methods

Nuclei isolation, solutions and patch, voltage clamp were described elsewhere (Bustamante, 1992, 1993). Sixteen male Swiss-Webster mice (20–22 g) were used. All experiments were conducted in nucleus-attached patches (i.e., the pipette tip was tightly sealed against the other surface of the NE). Nuclei were bathed in saline consisting of (mM): 150 KCl, 5 Hepes, 2.5 KOH (pH = 7.3–7.4). Patch pipettes were filled with this solution. Room temperature was chosen since physiological temperatures were considered a disadvantage to the analysis of channel conductance states. Under these conditions, the resting potential was negligible (Bustamante, 1992). Therefore, the actual potential across the nuclear envelope (V) was assumed to equal the potential applied to the Ag/AgCl electrode inside the patch-clamp pipette (the other Ag/AgCl electrode connected to the bath and set as reference, i.e., 0 mV). Sign convention for electrical currents is positive for outward currents and negative for inward currents. From previous studies, under control conditions the charge carrier for ion currents is K^+ (Bustamante, 1992, 1993). Therefore, outward currents represent outflow of K^+ from the nucleus (opposite for inward ion currents). Furthermore, it was previously shown that under these experimental conditions, the reversal potential for NIC currents (V_{rev}) is close to 0 mV, (Bustamante, 1992, 1993). Therefore, positive envelope potentials (negative pipette potentials) induced positive currents and vice versa.

Identity of main states and substates was strengthened by the following criteria (e.g., Hamill & Sakmann, 1981; Fox, 1987). (i) Transitions between main state and substate had to be observed, provided enough recording time was given to capture low probability states. (ii) Main states and substates had to share their ionic selectivity and pharmacological responses.

Each experiment lasted between 0.5 and 1 hr. Signals were filtered at 1 kHz (8-pole Bessel) prior to digitization. Data analysis was carried out with both commercial and custom, mixed-language computer software in an Intel-80386-based microcomputer (Bustamante, 1992, 1993). Where applicable, values are expressed as mean ± SD. An experiment was defined as the set of tests and results from a single NE patch. A total of 61 patches were studied.

Abbreviations and Symbols

i, electrical current-variable; NE, nuclear envelope; NIC, nuclear ion channel; NPC, nuclear pore complex; P, probability density function—variable; t, time—variable; τ, time constant—parameter or variable; T, dwell-time—parameter or variable; V, voltage—variable; V_{rev}, reversal potential—value of V at which i reverses direction; $\approx$, approximately equal; $\sim$, in the order of, closest numerical representation in base 10; 3-D, three-dimensional.

Results

Figure 1 illustrates changes induced in NIC current ($i(t)$) by a 65 sec voltage, V, pulse from 0 to +20 mV (top panel). The outward current signal was digitized at 100 μsec intervals. Time-expanded records of selected sections of the trace are shown below the top record on the left column. Plots of probability density function (P) *vs.* i are shown at the right of each expanded current record, i *vs.* time, t. P was obtained from the normalized current histograms (counts *vs.* current, 0.2 pA binwidth). From the P-i plots, one can appreciate the relative proportion of time the channel population spent in a particular conductance level or state. The expanded records on the left (bottom four) show brief sojourns to less than full (main) current transitions. As nuclear envelope potential, V, remained constant throughout the voltage pulse, these sojourns represent conductance state changes qualifying as subconductance levels.

Figure 1 shows that following application of a voltage pulse, the probability density function for current values, $P(i)$, shifted with time (i.e., $P = P(i,t)$) toward lower (quantized) levels of current. To illustrate this time-dependent change, a three-dimensional perspective of $P(i,t)$ surface was prepared for the time span of ≈120 sec (118.784 sec) as shown in Fig. 2 (time span determined by the file size limitations of the computer system hardware and software, *see* Bustamante, 1992, 1993). Consecutive cumulative amplitude histograms were obtained from the records at 4.096 sec intervals. Each histogram covered the same amount of time (i.e., 4.096 sec) and was exclusive of the other histograms. Since small current jumps were masked during this computational process (i.e., their contribution would be negligible to the cumulative histograms), the signal could be filtered without detriment of essential features. Thus, a 50 Hz-filter (digital Gauss algorithm of pCLAMP) was used to improve display of 3-D surfaces and to reduce the spurious 60 Hz line interference (for this particular experiment) whose main contribution was to broaden the peaks of the histograms. The binwidth in the histograms was set to 0.5 pA to reduce the number of operations during plotting (needed within the microcomputer environment used here). Figure 2 shows that the behavior of the ion channel population changed from an initial synchronous opening to a less ordinated, more purely random (binomial), mode of operation. A total of 51 patches responded within a millisecond to voltage pulse stimulation, the rest took seconds to activate. In all the 61 patches, the initial synchrony disappeared in time, as if the energy gained with the voltage pulse dissipated or as if channels inactivated (e.g., Bustamante, 1992). Putative states and substates were K^+ selective and were blocked by 100 mM Zn^{2+} and La^{3+} (Bustamante, 1993).

Figure 3 gives a portion of the experimental results and analysis obtained from a patch that displayed both fast and slow state transitions. The left-hand panels in Fig. 3 show current records, $i(t)$; their respective current probability density function, $P(i)$, are shown on the right. The current records correspond to the events that followed the initial 15 sec of the voltage pulse from V = 0 to +20 mV. Data for the initial 15 sec of the response were excluded from the analysis because it showed an activating behavior with a time constant of about 4 sec. (As mentioned, slow activation was seen in 16% of the 61 patches studied). The top ten current records are consecutive from top to bottom (total observation time of 40.96 sec). The records were digitized at 2 msec sampling intervals. During analysis, the data points were filtered at 25 Hz (Gauss algorithm) to reduce contribution of background noise to the histograms (*compare,* for example, with the increased standard deviation in the penultimate signal from top and its corresponding normalized histogram on its right). The two records at the bottom were sampled at 100 μsec and were not filtered during processing (i.e., bandwidth = 0–1 kHz, 8-pole Bessel, *see* Materials and Methods). These signals are important because they exemplify two major characteristics of channel state-transitions. First, NICs dwell in their main states for times in the order of 0.1–10 sec (Fig. 3, top ten records); however, short-lived sojourns are possible (Fig. 3, last record). Second, although transition times are well within a millisecond, some state-transitions (to and from the open state) seemed to require several milliseconds (Fig. 3, penultimate record from top). The plots of P *vs.* i were prepared by calculating the normalized histogram of the corresponding data record at the left with a binwidth of 0.2 pA. Thus, 2,048 and 500 data points were utilized to make, respectively, the top eleven and last P-i plots. These plots are given in a logarithmic scale to enhance the peaks at lower probability values. The last two records at the bottom demonstrate the relevance of frequency bandwidth to identifying channel states from histograms (e.g., time-resolution limitations may be countered by reducing the time window for fast responses as shown in the last record).

As for the experiment illustrated by Fig. 2, cumulative current histograms were computed for the top ten records, and the resulting probability density function, $P(i,t)$, was plotted as a function of time as shown in the 3-D surfaces of Fig. 4. Putative main states and substates can be appreciated in the two projection views of the $P(i,t)$ surface in Fig. 4. Similar to the features revealed by Fig. 2, the initial peaks of P, occurring at higher current values (equivalent to higher number of open channels), moved with time toward a region of lower current values (less number of channels open).

Three patches (out of the 61) displayed low-amplitude bursting activity. This activity was not accom-

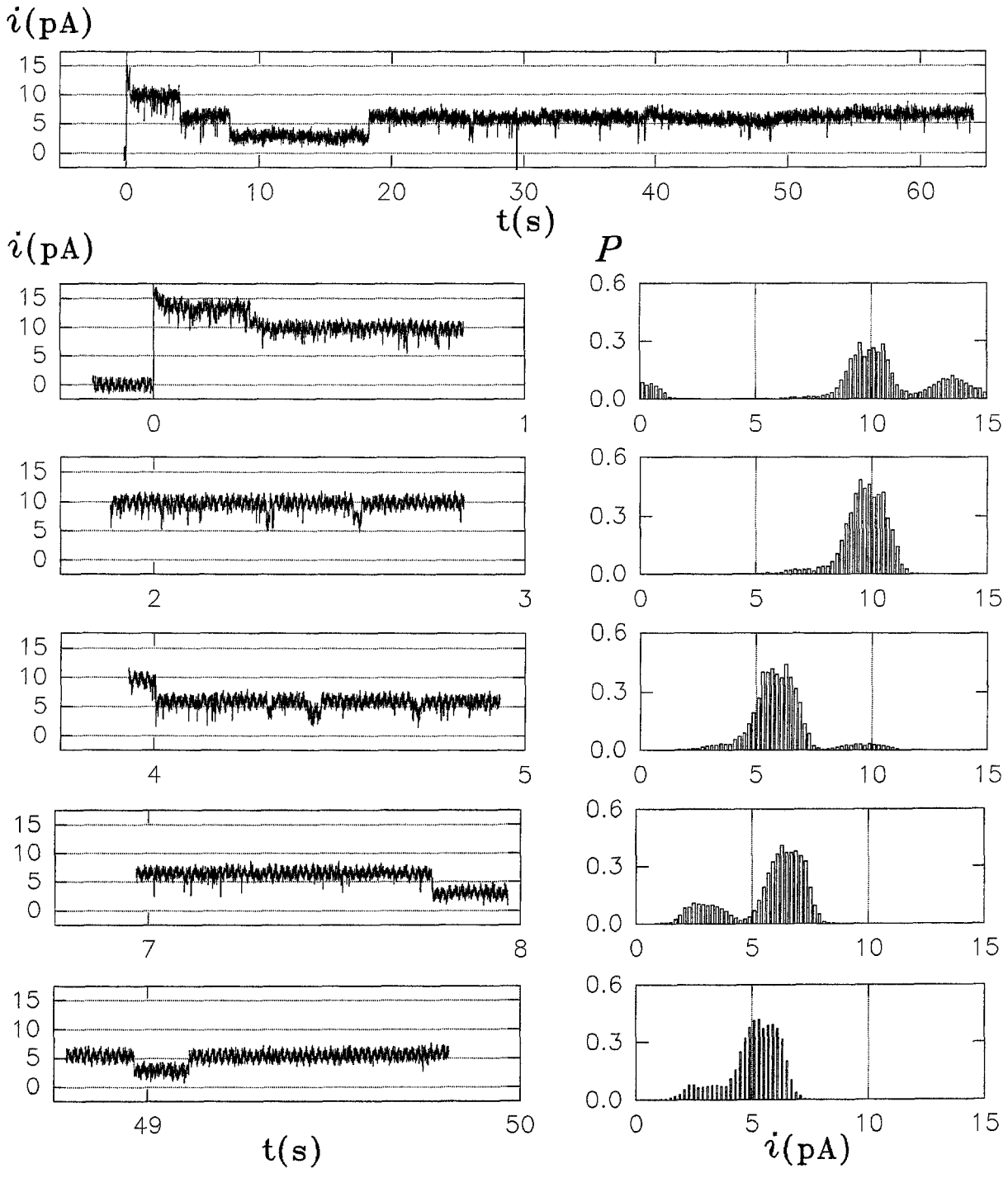

Fig. 1. *Top:* High-resolution, patch-clamp record of current signal response to a 65 sec envelope voltage pulse from 0 to +20 mV. The signal was digitized at 100 μsec intervals. *Bottom-left:* Time-expanded records of selected sections of signal at the top. Horizontal, time axis labels give the times corresponding to the record shown on top panel. *Bottom-right:* Plots of probability density function, *P, vs.* current, *i,* for the corresponding expanded current records on the left. *P* was obtained from the normalized current histograms (0.2 pA binwidth). A 60 Hz line interference contaminated the signals during this experiment but did not prevent analysis of essential features of the phenomenon studies.

panied by the typical, relatively large amplitude, stepwise activity shown so far (i.e., characteristic of nonbursting states and/or substates) and was taken to represent jumps from the closed state to an unfavored, putative subconductance state (despite the standard definition, e.g., Fox, 1987). Figure 5 illustrates one of these experiments. The top panel of Fig. 5 shows an 8 sec segment of a current record obtained at $V = +20$

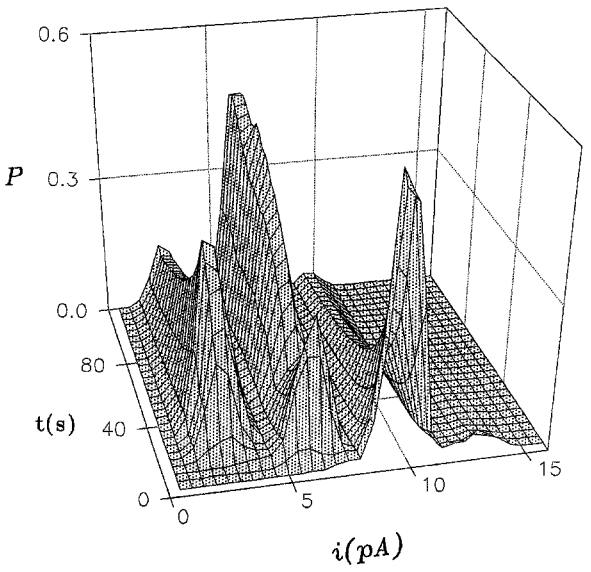

Fig. 2. Three-dimensional plot of the current probability density function $P(i)$ *vs.* time ($P = P(i,t)$) for the experiment illustrated in Fig. 1. Values of $P(i,t)$ were cumulative in time (time span of ≈120 sec). These values were obtained at 4.096 sec intervals from normalized, cumulative current histograms (counts *vs. i*, binwidth of 0.5 pA). During this computational process, small current jumps were masked and, therefore, filtering of the signal at 50 Hz did not affect the major features of the $P(i,t)$ surface but, instead, improved its appearance.

mV and digitized at 250 μsec. This particular segment of the record was chosen to give equal weight to both the closed and open states (i.e., 50% of the time the channel was in each state). To demonstrate the limitations of time resolution for analyzing these events, normalized current histograms (*P vs. i*, 0.2 pA binwidth) were calculated and plotted below the current record (top plot for all points, middle for the first 3.5 sec and the bottom for the last 3.5 sec). During the closed state the current was 12.4 ± 0.7 pA (calculated for the first 3.5 sec of the record). The current was 13.9 ± 1.2 pA during the open state (last 3.5 sec). Further analysis of this bursting channel activity was not conducted due to the proximity of the current levels for the close and open channel states. The phenomenon was taken as illustrating the fine workings of NIC function. That is, it is possible that normal NIC function was impaired and, as a result, this type of activity was unmasked.

Conductance states are usually deduced from exponential fits of closed and open dwell-times. Each component of the exponential fit is taken as being indicative of a singular state (e.g., Sakmann & Neher, 1983). Figure 6 depicts closed (shut) and open dwell-time histograms (top and bottom, respectively) for the experiment illustrated in Fig. 5. Event lists were prepared for the shut and open dwell-times with, respectively, 4.2 msec and 500 μsec binwidths (to accommodate the dwell-time range). A logarithmic scale was selected for the vertical axis to show the low probability readings of relatively long dwell-times (count of 1, top histogram). The baseline of 1 was subtracted in the calculation of the time constant for the shut state as it was thought to represent a different kinetic rate intractable due to the apparent reduced observation time which led to a constant value (equivalent to an infinite time constant). It may appear that the fits (superimposed, smooth unbroken lines) are not too tight, particularly for the shut dwell-times within the first 200 msec. However, this apparent misfit is due to the logarithmic scale (better looking fits yielded higher errors). Indeed, the percentage error (100 × SD/mean) for the time constant of the closed state (τ_{shut}) was only 7% (100 × 0.7/10). The percentage error for the open lines, with a time constant (τ_{open}) of 351 μsec, was 0.9% (100 × 3/351). Mean dwell-times for the shut and open states (T_{shut} and T_{open}) were, respectively, 21.8 msec and 671 μsec. These represent the inverse of the sum of transition rates leading away from the state (e.g., Sakmann & Neher, 1983). The τ and T calculated for the three patches where bursting activity was observed were: $\tau_{shut} = 23.1 \pm 12.9$ msec, $\tau_{open} = 371 \pm$ μsec, $T_{shut} = 32.3 \pm 16.7$ msec and $T_{open} = 435 \pm 172$ μsec. These wide ranges of τ and T parallel the wide range of values observed for single nuclear channel conductance (between 100 and 500 pS, *see* Bustamante, 1992).

Dwell-time histograms for the typical channel behavior of stepwise current jumps (55 out of 61 channels) were difficult to construct since all patches contained more than one functional channel. Only two patches contained two channels and the rest contained from 3 to 18 operational channels (calculated by counting the maximum number of discrete and similar current jumps). This observation is in agreement with the high density of nuclear pores per envelope unit area (*see* Mazzanti et al., 1991; Bustamante, 1994). Therefore, the analysis of dwell-times was limited to these two experiments and, thus, the results must be taken only as indicative of the order of magnitude of the values calculated. Figure 7 illustrates the dwell-time histograms for the closed state (top panel), and for the two open state levels (*open1* and *open2*) presumed to result from two active channels (second and third panels from top). The binwidth in the dwell-time histograms was set to 2 msec due to the large spread of time values. The horizontal scale is logarithmic to cover the wide span of values observed. The normalized current histogram (*P vs. i*, binwidth of 0.5 pA) is given on the bottom panel to demonstrate the presence of the three major current levels (i.e., the three histogram peaks). The calculated values for the time constants, τ, of the exponential fits (insets in each histogram) show the large errors (SD) that resulted. Superimposed on the histogram bars are the smooth continuous lines corresponding to the fits. On the assumption that the lower peak of the current histogram in Fig. 7 corresponds to the closed state, then

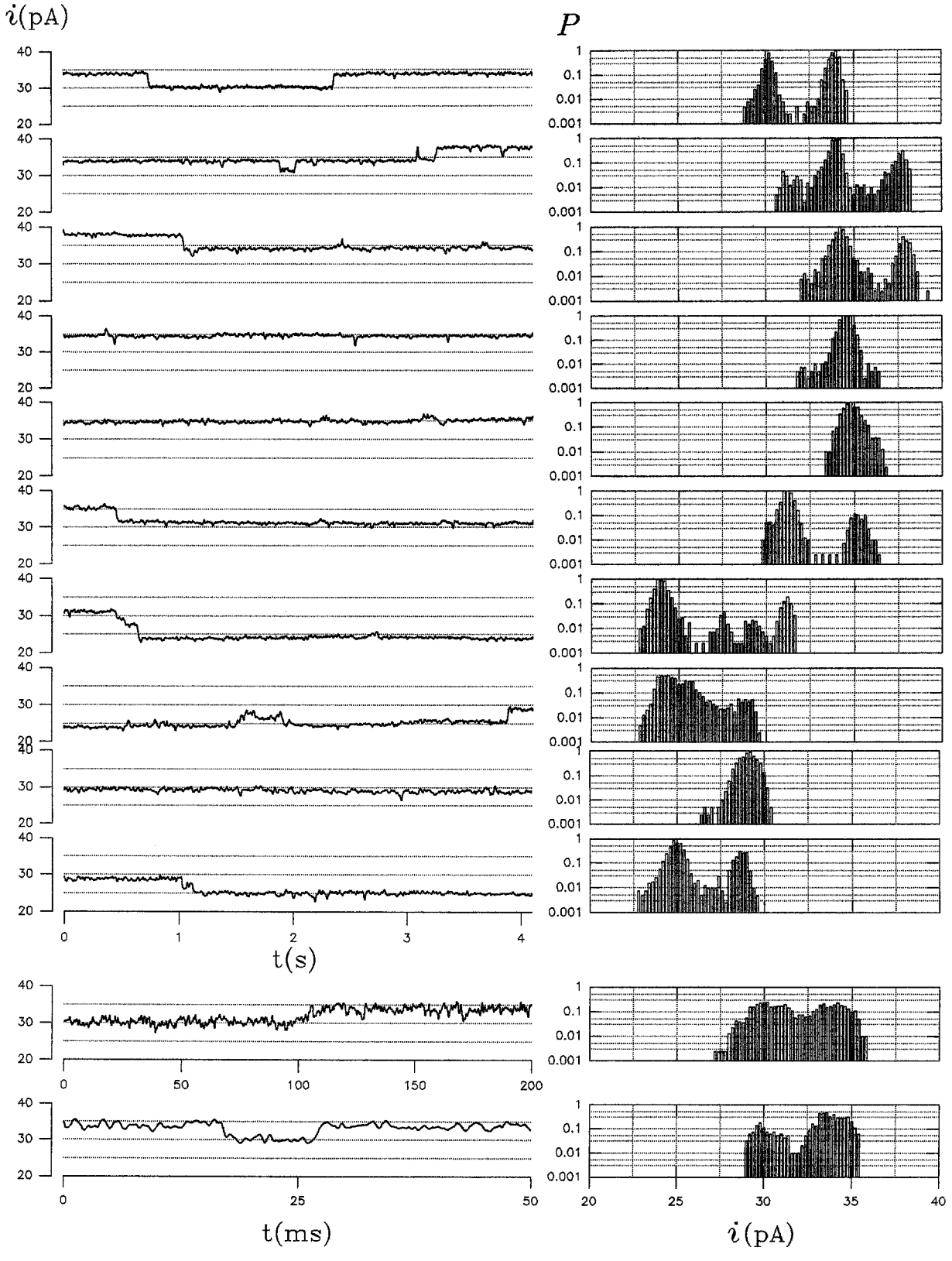
i(pA)
P
t(s)
t(ms)
i(pA)

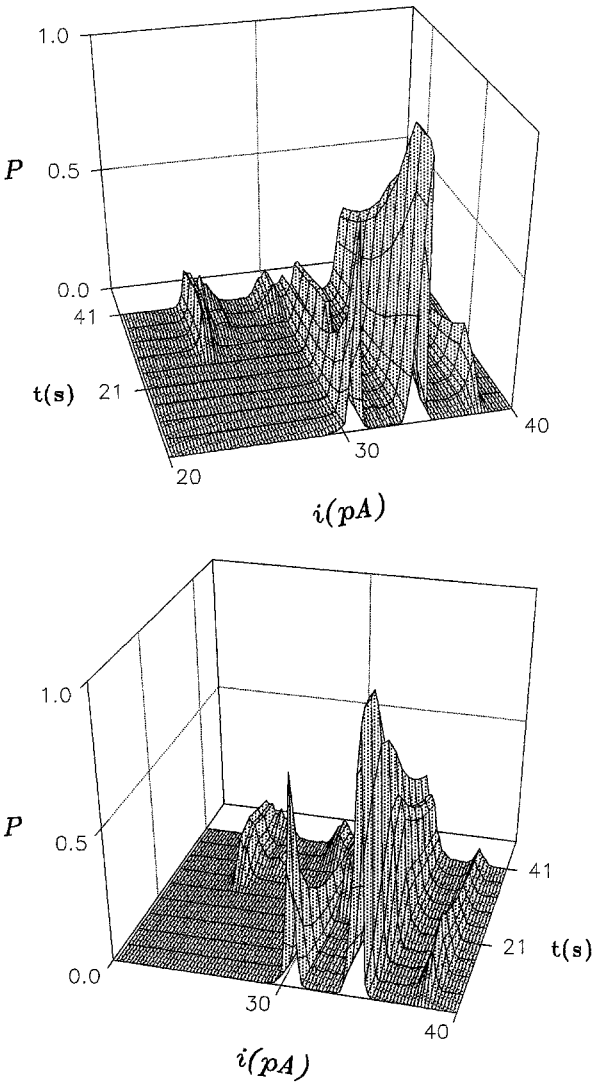

Fig. 4. Plot of cumulative current probability density function *vs.* time, $P(i,t)$, drawn from the top ten records of Fig. 3. The top and bottom panels represent two different views of the same $P(i,t)$ surface. Similar to the features seen in Fig. 2, the initial peaks of P at higher current values (i.e., higher number of open channels) are seen to move with time toward a region of lower (less channels open).

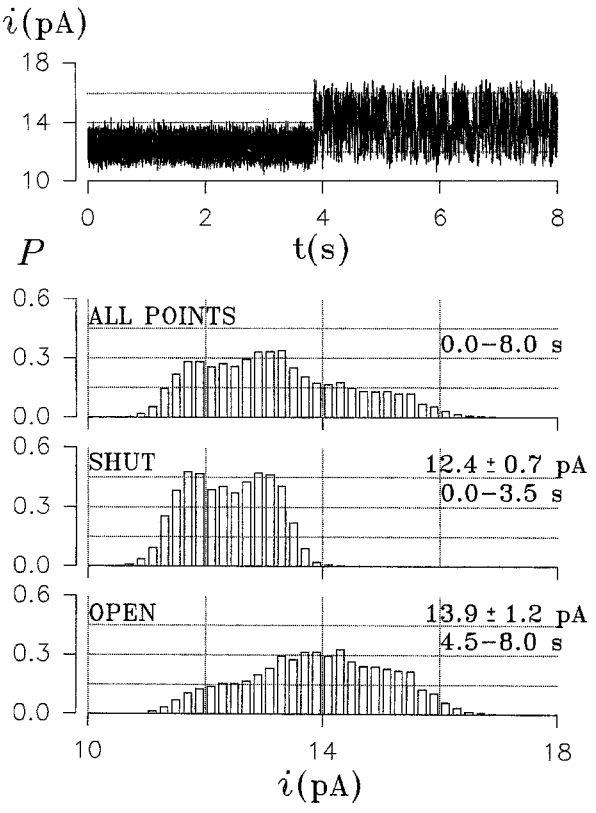

Fig. 5. Low-amplitude, high-bursting frequency nuclear channel activity at +20 mV of nuclear envelope potential. The points in the top current record were obtained with a 250 μsec sampling interval. Normalized current probability histograms (P *vs.* i, 0.2 pA binwidth) are given below the top current record. The top histogram was calculated with all the current record points (*ALL*). The middle histogram was calculated with the first 3.5 sec of the record which comprised only the closed-state values (*SHUT*). The bottom histogram was prepared with the last 3.5 sec of the record, thus containing only the sampled burst (*OPEN*).

one may conclude that the patch contained only two functional channels. If one then assumes that the channels are identical and independent of each other, then one could make the approximation that there is a contribution of 50% from each of these channels to the measured open dwell-times for level 1 (open1). Likewise, the time spent in the closed level must have been underestimated by half due to the sojourns by the two channels. Thus, τ_{shut} and τ_{open1} can be approximated, respectively, as twice and half the values obtained (i.e., about 160 and 40 msec each). The mean shut and open dwell-times calculated from the histograms were T_{shut} = 161.1 msec, T_{open1} = 564.7 msec and T_{open2} = 61.4 msec. In the other two-channel patch analyzed, the values calculated for τ_{shut} and τ_{open1} were 120 ± 54 msec

Fig. 3. Part of a current response to a +20 mV voltage pulse delivered from a basal level of 0 mV. *Left:* Current records, $i(t)$. *Right:* Noncumulative probability density functions, $P(i)$, corresponding to the current records on the left (0.2 pA binwidth). A logarithmic scale was used to enhance the events that took place at lower probabilities. The initial 15 sec section following the voltage pulse was excluded from the analysis because it showed an activating behavior (time constant of about 4 sec). Top ten, current records are consecutive from top to bottom. The records were obtained with a 2 msec sampling interval and were filtered during analysis at 25 Hz (Gauss algorithm) to reduce contribution of background noise to the P (i) plots. The two records at the bottom were obtained with a 100 μsec sampling interval, no further filtering was applied during analysis (i.e., signal bandwidth = 1 kHz, corresponding to the 8-pole Bessel filtering of raw signals, *see* Materials and Methods).

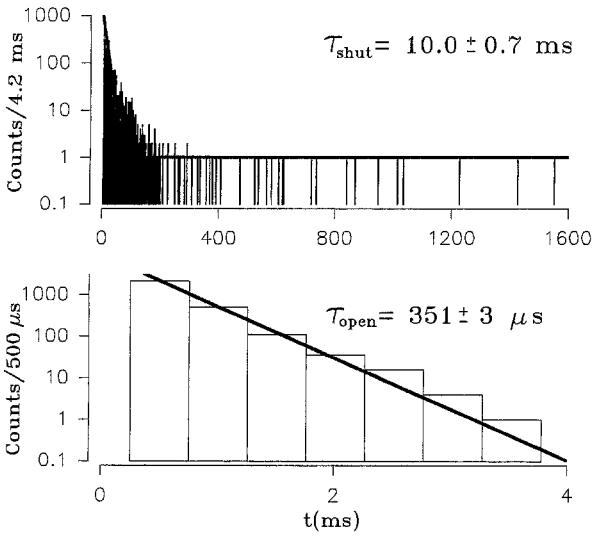

Fig. 6. Shut (closed) and open dwell-time histograms (top and bottom, respectively) for the low-amplitude, high-frequency activity of the experiment illustrated in Fig. 5. The continuous lines superimposed on the histograms were drawn according to the mono-exponential parameters calculated from a nonlinear regression fit (values given in each plot). The baseline of 1 for the shut dwell-time histogram was taken to represent a long-lasting closed state unresolved within the observation time scale.

and 142 ± 37 msec, respectively. T_{shut} and T_{open1}, T_{open2} were about 193, 480 and 45 msec, respectively. The top two dwell-time histograms of Fig. 7 show a one-count component that suggests a very slow process which could not be resolved within the observation time because it seems to have time constants much larger than 10 sec. As mentioned above, there were not enough data to make a statistically significant estimate. However, the analysis helped in estimating the order of magnitude of the parameters characterizing the process, thus allowing prediction of potential correlations to nuclear processes.

On the basis of their identical reversal potentials ($V_{rev} \approx 0$ mV), all conductance states reflected similar selectivity. This is best illustrated by the current responses to voltage ramps as shown in Fig. 8. The left panel in Fig. 8 shows five current records (*i vs. t*) selected from an ensemble of 30, elicited by 10 sec ramps separated by 20 sec intervals. The voltage range covered by the ramps was ±40 mV. The signals were filtered at 100 Hz and digitized at 5 msec intervals. The voltage dependence of channel conductance is shown with the patch conductance *vs.* voltage plots (*i/V vs. V*) on the right of Fig. 8. These plots were obtained after dividing the current signal at the left by the delivered voltage. Artifacts around $V = 0$ mV are apparent. These were due to small errors magnified during division by very small numbers (i.e., when $i \neq 0$ pA and $V \approx 0$ mV). As shown previously (e.g., Bustamante, 1992), NIC conductance is linear. Calculated conduc-

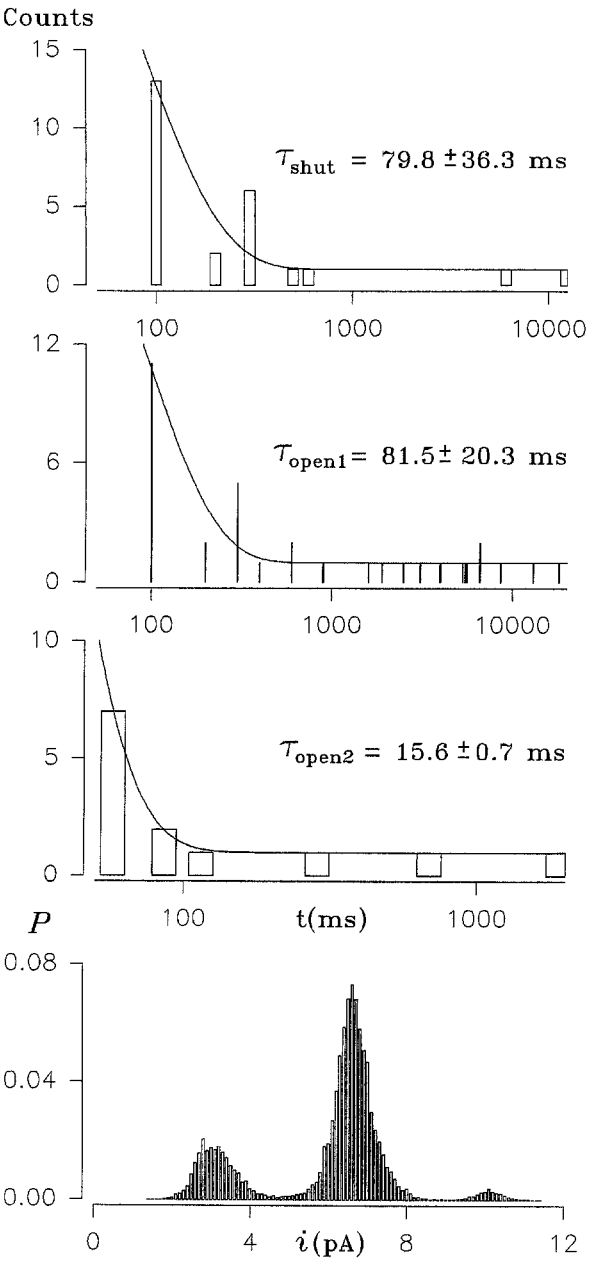

Fig. 7. Histograms of dwell-time and current (top three and bottom panels, respectively) for typical nuclear channel behavior in a two-channel patch. Logarithmic scales were used in horizontal axes to cover the range of measurements. Top panel corresponds to the closed state. Below the top panel are the histograms for the two putative open states, open1 and open2, presumed to result from two active channels. Binwidth in dwell-time histograms was 2 msec. The normalized current histogram, *P vs. i* (0.5 pA binwidth) is given on the bottom panel to demonstrate the three major current levels (from left to right: closed, open1 and open2). Calculated time constants, τ, of the exponential fits are shown in the histogram insets. The continuous lines superimposed on the dwell-time histograms were drawn according to the parameter found with the curve-fitting procedures.

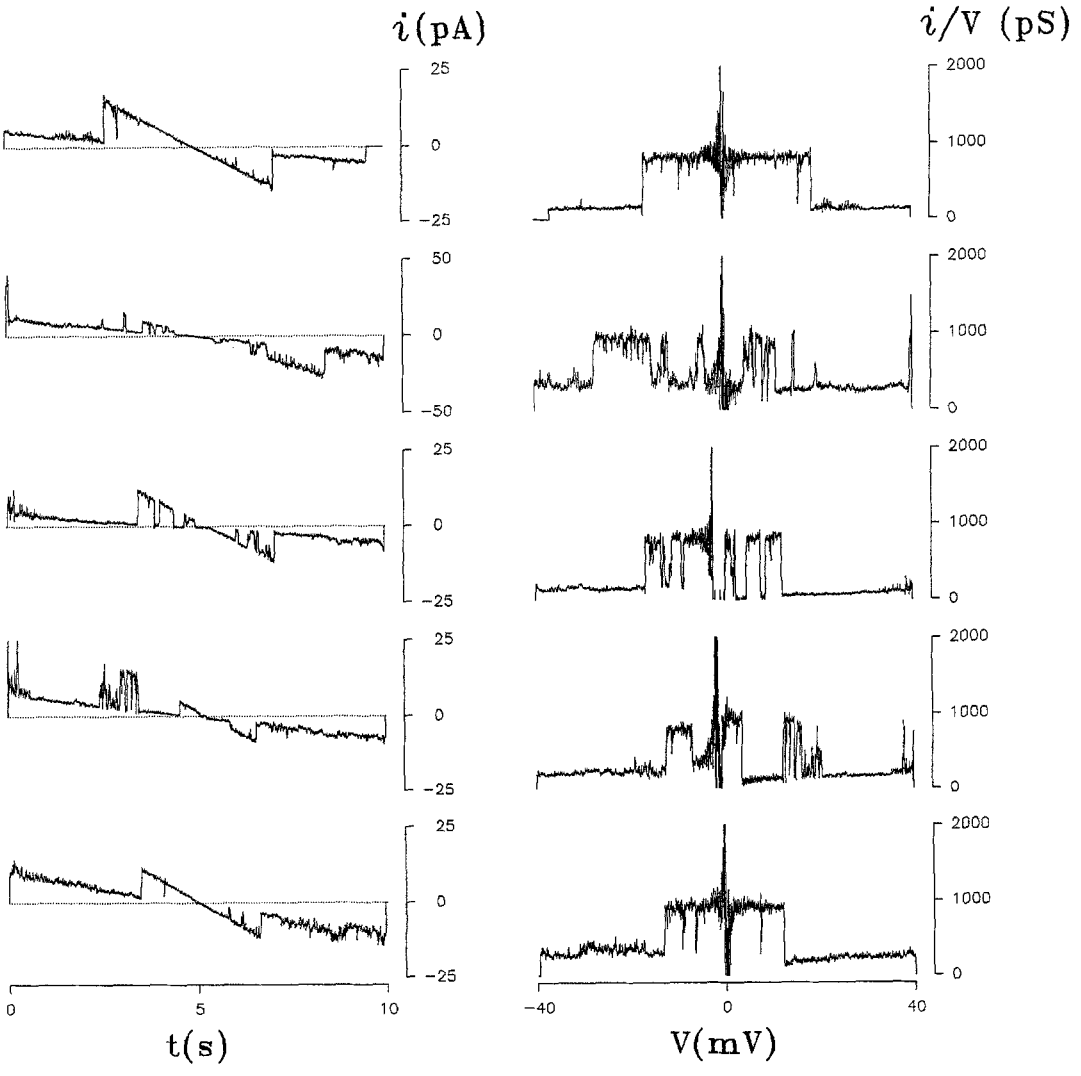

Fig. 8. *Left:* Current responses, $i(t)$, to ±40 mV, 10 sec voltage ramps separated by 20 sec intervals. The records were selected from an ensemble of 30 signals. The signals were filtered at 100 Hz and digitized at 5 msec intervals. *Right:* Plots of patch conductance, *i/V, vs.* envelope patch voltage, *V*, were computed from the current records shown on the left by dividing their values by the corresponding voltage-ramp voltage. At $V = 0$ mV, artifacts resulted due to the several-fold amplifications produced by division of small numbers by much smaller numbers (*see* Bustamante, 1994).

tance values for main states and substates (obtained from voltage ramp and voltage pulse protocols) ranged, respectively, between 120 and 490 pS (281 ± 198, pS, $n = 55$) and 25 and 50 pS (37 ± 11 pS, $n = 6$).

Finally, it was only after long periods of observation (~1–10 min) that apparently inactive patches demonstrated activity of the type discussed above ($n = 8$). That is, it took several minutes to decide that a patch actually had the capability of excitation or that the measured baseline current detected was not an electrode-polarization artifact. This phenomenon was taken to indicate that several unknown forces influence NIC activity and that these forces determine that NICs dwell in either open or closed states for very long periods of time (~1–10 min).

Discussion

The results from patches containing several channels can be interpreted within the framework of the binomial distribution (*see* Bustamante, 1992, and references therein):

$$P(m) = \frac{N!}{m!(N-m)!} p^m (1-p)^{N-m} \qquad (1)$$

where N is the total number of channels, m is the number of channels open, p is the probability of opening for a single channel, and P is the probability of finding m channels open (equivalent to the above definition). Bearing in mind that the binomial model assumes iden-

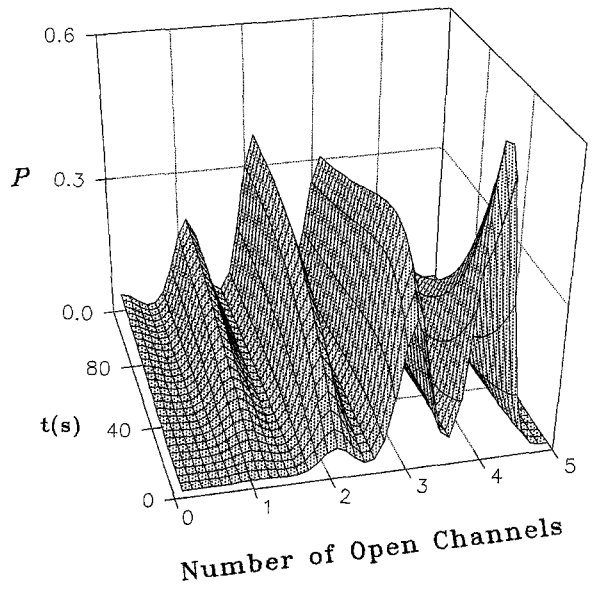

Fig. 9. Time course of simulated binomial distributions probability function, P, for a population of four channels whose single-channel probability of being open, p, decays exponentially from an initial value of 0.9 to a final value of 0.5 with a time constant of about 59.4 sec (half the observation time of Fig. 2). A Gaussian distribution with a standard deviation of 0.2 units was applied to each calculated probability to better simulate the experimental data.

tical and independent functional units (*see* Bustamante, 1992), one can make the following interpretation. Prior to stimulation (e.g., $t < 0$ sec in Figs. 1 and 2), the system is in equilibrium at $V = 0$ mV (i.e., sufficient time elapsed to allow system equilibration). Since under control conditions no electrochemical gradient exists (equal to $V - V_{rev}$, with $V = V_{rev} = 0$ mV) to drive the electrical charge carriers (K^+ ions) across open channels, it is difficult to ascertain whether at this null electrochemical gradient there are channels opening and closing (this, however, does not preclude our discussion). Upon transition from $V = 0$ mV to $V \neq 0$ mV (e.g., $V = +20$ mV at $t \geq 0$ sec in Figs. 1 and 2), there is a net force driving the ions through NIC openings. That the current histograms are not symmetrical (but thrown toward higher values of current) shortly after the stimulus is an indication that the probability of single channel opening, p, is modified (toward higher values). As time passes, the system adapts to the new condition and it is able to reach a new equilibrium state, where the probability of opening for each channel, p, equals that of closing (1-p, i.e., 0.5). Figure 9 illustrates the time course of predicted binomial distributions for a population of four independent channels (i.e., $N = 4$) whose variable p changes exponentially in time, t, according to the following phenomenological formula (solution to a simple, homogeneous, differential equation describing a two-state system):

$$p(t) = p_\infty + (p_0 - p_\infty)\, e^{-t/\tau} \qquad \text{(a)}$$

where p_∞ is the final steady-state value attained by p (i.e., 0.5), p_0 is the initial ($t = 0$ sec) value reached by p upon stimulation (assumed here to be a maximum of 0.9), and t is the time constant (assumed to be half the observation time of Fig. 2 or 59.392 sec). A Gaussian distribution with standard deviation of 0.2 channel units (to simulate the actual histograms prepared from the current recordings) was applied to each value of $P(m)$ calculated from the binomial distribution. From Fig. 9 one may conclude that a process more complex than assumed in this simulation must have taken place in reality. The exponential decay model of p was based on the previous finding that nuclear ion channels may display exponential inactivation (Bustamante, 1992). Other approaches may be used in describing the observations illustrated by Figs. 1 and 2. For example, one could have combined two sets of channels: inactivating and noninactivating (e.g., Bustamante, 1992). Regardless of the model used to describe or predict the time-dependent change in P, one may conclude from the experimental results alone that voltage pulses evoked synchronized NIC openings and that a few seconds after, the channels became less synchronous in their operation (as expected from a truly random process left to equilibrate—i.e., the initially reduced entropy, increased as time progressed). This operation may be relevant to nucleocytoplasmic transport in that it may represent a feedback mechanism by which the channel population is alerted of sudden changes in the environment but accommodates with time. That is, initially, all channels are put to work; in the end, only half of them do the work per unit time.

Implicit in their definition is that main states are favored by their higher probability of occupancy. The results presented in this paper demonstrate that a kinetic diagram of NIC function must consist of at least three closed states and two open states. The dwell-times for the closed states were in the order of tens of milliseconds (e.g., Fig. 6, putative substate), hundreds of milliseconds (e.g., Fig. 7) and more than 10 sec (e.g., Fig. 7). Submillisecond open dwell-times were observed for a putative substate (e.g., Fig. 6) while open dwell-times of tens of milliseconds were also observed (e.g., Fig. 7). Eight patches showed that NICs could dwell for many minutes in either the closed or open states. These extremely long open and closed dwell-times (~min) add at least two more states although other models may be considered (e.g., modulatory levers correlated to phosphorylation, *see* Bustamante, 1992). Previous investigations with channel blockers and ion substitution have helped uncover these extremely long dwell-times (Bustamante, 1994). For example, apparently inactive NICs (i.e., constant current) may be demonstrated to be fully active (open) by K^+ substitution (e.g., tetraethylammonium), after which manipulation,. transitions to closed states are detected. Therefore, a third open state must be included in the NIC functional diagram.

Direct inspection of the current records revealed

open states of low amplitude and high frequency (e.g., record in Fig. 5). As the chance of observing these low-amplitude events by themselves (i.e., independently of the most common main states) was relatively low (3 out of 61 patches or about 5%), it may be concluded that these are a manifestation of open states of low probability and candidates for the denomination of substates (although according to Fox, 1987, their independent operation may invalidate this classification).

The ideas presented here are based on the fact that nuclear pore complexes, NPCs, are the likely physical substrate for NICs (e.g., Mazzanti et al., 1990, 1991; Bustamante, 1992; Matzke et al., 1992) and on current concepts of NPC structure with a centrally located plug connected to eight radial spokes; a plug that gates "open" and "closed" the NPCs (e.g., Akey, 1989, 1990, 1991, 1992; Akey & Goldfarb, 1989; Dingwall, 1990, 1991; Reichelt et al., 1990; Jarnik & Aebi, 1991; Hinshaw et al., 1992; Akey & Radermacher, 1993). An interesting observation made during the present experiments was that of slow transitions times (>msec), a phenomenon shared with gap junctional channels (e.g., Neyton & Trautmann, 1985). Since no plug has been detected for gap junctional channels, it is hard to put forward the attractive argument that the slow NIC transition times are correlated to hypothetical sluggish displacements of the large mass and dimension of the central NPC plug (12.0 ± 1.1 MD, Reichelt et al., 1990). Other structural features of NPCs may be exploited to explain NIC activity observed in the current studies. Possible candidates are the radial spokes of the NPCs. However, spoke mass was found to be even higher than that of the central plug (51.7 ± 5.3 MD, Reichelt et al., 1990). Therefore, other mechanisms may be acting in the two types of channels or if they were the same then there seems to be no role for a megaplug. The eight small channels peripheral and parallel to the large central channel of the NPC (Hinshaw et al., 1992) could not be confirmed in a recent study (Akey & Radermacher, 1993). Furthermore, atomic force microscopy of putatively intact nuclear envelopes of *Xenopus laevis* oocytes failed to show the large central channel of the NPCs (Panté, Goldie & Aebi, 1993), an indication that much work remains to be done before a clear picture of the living NPC is attained. Further discussion of this topic is outside the scope of this paper.

The data presented here were obtained from nuclei bathed in nominally saline solutions. Under these conditions, it would seem unlikely that macromolecular exchange across the envelope would have taken place (e.g., Bustamante, 1994). Therefore, one may reach the conclusion that the data presented here have little significance to macromolecular transport (e.g., proteins) because it is known that cytosolic factors must be present for transport of large molecules (*reviewed in* Bustamante, 1994). That this is not the case for the present experiments is supported by recent experiments by this investigator demonstrating that adult cardiac myocyte NICs cannot open under pure saline conditions (*see* Fig. 1 in Bustamante, 1994). Therefore, as originally discussed (Bustamante, 1992), one must conclude that since the isolated nuclei used in these experiments were not separated from cell debris but kept in the cell lysate, bath perfusion did not effect sufficient washout of these important cytosolic substrates (due to the relatively large size of the bath used in these experiments— ≈1 ml compared to ≈0.1 ml of the bath used in recent experiments). Furthermore, one may extrapolate that NIC inactivation may reflect an intermediate state resulting from limited and less than optimal supply of cytosolic factors. Thus, the one or more inactivation time constants describing the kinetics of the transient should reflect the stability of the system, with the final state attained upon excitation being the stable state. The kinetic parameters of the process are probably determined by the cytosolic factors known to affect nucleocytoplasmic transport. Ligands to the nuclear pore, such as nuclear localization signals or their cytosolic receptors (*see* Bustamante, 1994), may play a major role in determining the presence and/or magnitude of NIC inactivation.

Consequently, with cautious optimism one may say that the observations presented here are relevant to macromolecular transport should NICs be proven to be NPCs or parts thereof. Substance for this statement comes from recent data demonstrating, for the first time, that protein transport is depressed by GTPγS, a nonhydrolyzable analogue to GTP (Marshallsay & Lührmann, 1993; Melchior et al., 1993; Moore & Blobel, 1993), an effect previously demonstrated for cardiac NICs (Bustamante, 1994).

Following the rationale presented for putative protein-conducting channels of the endoplasmic reticulum (Simon & Blobel, 1991, 1992) one must conclude that NIC currents must represent ion transport through open NPCs that do not conduct macromolecules, for otherwise the pores would have been plugged. That is, under this paradigm only NIC closed states should represent macromolecular translocation (provided that the cytosolic requirements are present), an idea that, without being antagonic, would be the converse of the theory for ion conduction through ion channels.

The field of nuclear envelope ion channels is hardly explored and, knowing the complexity of nuclear function, it should not be surprising to find out in future investigations, that NIC activity is influenced (directly or indirectly) by many factors involved in macromolecular transport (e.g., "cytosolic factors"), nuclear function (e.g., protein kinases and phosphatases, ribonucleotides, and nucleic acid polymerases), etc. Demonstration of the merit of nuclear electrophysiology in evaluating various aspects of nuclear function, inclusive of nucleocytoplasmic transport, remains a challenging topic of investigation (*see* Bustamante, 1994). Until the identity of NICs with NPCs is demonstrated, it seems appropriate (in practice and theory) to keep the elec-

trophysiological concept apart from the structural one. As previously discussed (Bustamante, 1992, 1993*a,b*), NPC antibodies should prove essential in resolving NIC identity to NPCs.

Finally, the current studies were carried out with nuclei from adult cardiac myocytes. Reasons for the choice of a preparation of committed, differentiated cells were given in the introduction. Studies of nuclear pore structure and of nucleo-cytoplasmic transport of macromolecules have been carried out in gamete or cultured cells (e.g., respectively: Akey & Radermacher, 1993; and Adam, Sterne-Marr & Gerace, 1991*a,b*). It is now clear that cell type is an important determinant of the requirements for transport of large and small proteins (e.g., Marshallsay & Lührmann, 1993). Therefore, complete interpretation of the data presented here with data collected from nonelectrophysiological studies of macromolecular transport, and *vice versa,* may not be warranted. Each data set may intercept or partially superimpose each other.

This work is supported by the American Heart Association, Maryland Affiliate. The author extends his gratitude to Dr. Louis J. DeFelice for his frank, critical review of the original manuscript.

References

Adam, S.A., Sterne-Marr, R., Gerace, L. 1991*a*. *In vitro* nuclear protein import using permeabilized mammalian cells. *Methods Cell Biol.* **35**:469–482

Adam, S.A., Sterne-Marr, R., Gerace, L. 1991*b*. Nuclear protein import in permeabilized mammalian cells requires soluble cytoplasmic factors. *J. Cell Biol.* **111**:807–816

Akey, C.W. 1989. Interactions and structure of the nuclear pore complex revealed by cryo-electron microscopy. *J. Cell Biol.* **109**:955–970

Akey, C.W. 1990. Visualization of transport-related configurations of the nuclear pore transporter. *Biophys. J.* **58**:341–355

Akey, C.W. 1991. Probing the structure and function of the nuclear pore complex. *Semin. Cell Biol.* **2**:167–177

Akey, C.W. 1992. The nuclear pore complex. *Curr. Opin. Struct. Biol.* **2**:258–263

Akey, C.W., Goldfarb, D.S. 1989. Protein import through the nuclear pore complex is a multistep process. *J. Cell Biol.* **109**:971–982

Akey, C.W., Radermacher, M. 1993. Architecture of the *Xenopus* nuclear pore complex revealed by three-dimensional cryo-electron microscopy. *J. Cell Biol.* **122**:1–19

Boer, P.H., de Bold, M.L., de Bold, A.J., Bustamante, J.O. 1991. Activation mode of the atrial natriuretic factor gene during P19 cardiac myogenesis. *FASEB J.* **5**:A1748

Burt, J.M., Spray, D.C. 1988. Single-channel events and gating behavior of the cardiac gap junction channel. *Proc. Natl. Acad. Sci. USA* **85**:3431–3434

Bustamante, J.O. 1992. Nuclear ion channels in cardiac mycoytes. *Pfluegers Arch.* **421**:473–485

Bustamante, J.O. 1993. Restricted ion flow at the nuclear envelope of cardiac myocytes. *Biophys. J.* **64**:1735–1749

Bustamante, J.O. 1994. Nuclear electrophysiology. *J. Membrane Biol.* **138**:105–112

Bustamante, J.O., McDonald, T.F. 1983. Sodium currents in segments of human heart cells. *Science* **220**:320–321

Bustamante, J.O., Ruknudin, A., Sachs, F. 1991. Stretch-activated channels in heart cells: relevance to cardiac hypertrophy. *J. Cardiovasc. Pharmacol.* **17**:S110–S113

Bustamante, J.O., Watanabe, T., McDonald, T.F. 1981. Single cells from adult mammalian heart: Isolation procedure and preliminary electrophysiological studies. *Can. J. Physiol. Pharmacol.* **59**:907–910

Bustamante, J.O., Watanabe, T., McDonald, T.F. 1982. Non-specific proteases: a new approach to the isolation of adult cardiocytes. *Can. J. Physiol. Pharmacol.* **60**:997–1002

Bustamante, J.O., Watanabe, T., Murphy, T.F., McDonald, T.F. 1982. Isolation of single atrial and ventricular cells from the human heart. *Can. Med. Assoc. J.* **126**:791–793

Davis, L.I. 1992. Control of nucleocytoplasmic transport. *Curr. Opin. Cell. Biol.* **4**:424–429

Dingwall, C. 1990. Plugging the nuclear pore. *Nature* **346**:512–514

Dingwall, C. 1991. Transport across the nuclear envelope: enigmas and explanations. *BioEssays* **13**:213–218

Fox, J.A. 1987. Ion channel subconductance states. *J. Membrane Biol.* **97**:1–8

Hamill, O.P., Sakmann, B. 1981. Multiple conductance states of single acetylcholine receptor channels in embryonic muscle cells. *Nature* **294**:462–464

Hanover, J.A. 1992. The nuclear pore: at the crossroads. *FASEB J.* **6**:2288–2295

Hernández-Cruz A., Sala, F., Adams, P.R. 1990. Subcellular calcium transients visualized by confocal microscopy in a voltage-clamped vertebrate neuron. *Science* **247**:858–862

Hernández-Cruz, A., Sala, F., Connor, J.A. 1991. Stimulus-induced nuclear Ca^{2+} signals in fura-2-loaded amphibian neurons. *Ann. NY Acad. Sci.* **635**:416–420

Hinshaw, J.E., Carragher, B.O., Milligan, R.A. 1992. Architecture and design of the nuclear pore complex. *Cell* **69**:1133–1141

Innocenti, B., Mazzanti, M. 1993. Identification of a nucleo-cytoplasmic ionic pathway by osmotic shock in isolated mouse liver nuclei. *J. Membrane Biol.* **131**:137–142

Jarnik, M., Aebi, U. 1991. Toward a more complete 3-D structure of the nuclear pore complex. *J. Struct. Biol.* **107**:291–308

Karin, M. 1991. Signal transduction and gene control. *Curr. Opin. Cell Biol.* **3**:467–473

Loewenstein, W.R. 1981. Junctional intercellular communication: the cell-to-cell membrane channel. *Physiol. Rev.* **61**:829–913

Loewenstein, W.R., Kanno, Y. 1962. Some electrical properties of the membrane of a cell nucleus. *Nature* **195**:462–464

Loewenstein, W.R., Kanno, Y., Socolar, S.J. 1978. Quantum jumps of conductance during formation of membrane channels at cell-cell junction. *Nature* **274**:133–136

Manivannan, K., Ramanan, S.V., Mathias, R.T., Brink, P.R. 1992. Multichannel recordings from membranes which contain gap junctions. *Biophys. J.* **61**:216–227

Marshallsay, C., Lührmann, R. 1993. In vitro nuclear import of snRNPS: cytosolic factors mediate m3g-cap dependence of U1 and U2 snRNP transport. *In:* Programme and Abstracts of The International Symposium on RNA Processing and Nucleo-Cytoplasmic Transport. p. 27. Marburg, Germany

Matzke, A.J.M., Behensky, C., Weiger, T., Matzke, M.A. 1992. A large conductance ion channel in the nuclear envelope of a higher plant cell. *FEBS Lett.* **302**:81–85

Matzke, M.A., Matzke, A.J.M. 1986. Visualization of mitochondria and nuclei in living plant cells by the use of a potential-sensitive fluorescent dye. *Plant Cell Environ.* **9**:73–77

Matzke, A.J.M., Matzke, M.A. 1991. The electrical properties of the nuclear envelope and their possible role in the regulation of eukaryotic gene expression. *Bioelectrochem. Bioenerg.* **25:**357–370

Matzke, M.A., Matzke, A.J.M., Neuhaus, G. 1988. Cell age-related differences in the interaction of a potential-sensitive fluorescent dye with nuclear envelopes of *Acetabularia mediterranea*. *Plant Cell Environ.* **11:**157–163

Matzke, A.J.M., Weiger, T.M., Matzke, M.A. 1990. Detection of a large cation-selective channel in nuclear envelopes of avian erythrocytes. *FEBS Lett.* **271:**161–164

Mazzanti, M., DeFelice, L.J., Cohen, J., Malter, H. 1990. Ion channels in the nuclear envelope. *Nature* **343:**764–767

Mazzanti, M., DeFelice, L.J., Smith, E.F. 1991. Ion channels in murine nuclei during early developments and in fully differentiated adult cells. *J. Membrane Biol.* **121:**189–198

Melchior, F., Paschal, B., Guan, T., Gerace, L. 1993. Biochemical analysis of nuclear protein import. *In:* Programme and Abstracts of The International Symposium on RNA Processing and Nucleo-Cytoplasmic Transport. p. 23. Marburg, Germany

Moore, M., Biobel, G. 1993. Two distinct cytosolic factors required for nuclear import. *In:* Programme and Abstracts of The International Symposium on RNA Processing and Nucleo-Cytoplasmic Transport. p. 24. Marburg, Germany

Neylon, C.B., Hoyland, J.M., Mason, W.T., Irvine, R. 1990. Spatial dynamics of intracellular calcium in agonist stimulated vascular smooth muscle cells. *Am. J. Physiol.* **259:**C675–C686

Neyton, J., Trautmann, A. 1985. Single-channel currents of an intercellular junction. *Nature* **317:**331–335

Nigg, E.A., Baeuerle, P.A., Lührmann, R. 1991. Nuclear import-export: in search of signals and mechanisms. *Cell* **66:**15–22

Panté, N., Goldie, K.N., Aebi, U. 1993. Towards a molecular understanding of the nuclear pore complex structure and function. *In:* Programme and Abstracts of The International Symposium on RNA Processing and Nucleo-Cytoplasmic Transport. pp. 15–16. Marburg, Germany

Przywara, D.A., Bhave, S.V., Bhave, A., Wakade, T.D., Wakade, A.R. 1991. Stimulated rise in neuronal calcium is faster and greater in the nucleus than in the cytosol. *FASEB J.* **5:**217–222

Reichelt, R., Holzenburg, A., Buhle, Jr., E.L., Jarnik, M., Engel, A., Aebi, U. 1990. Correlation between structure and mass distribution of the nuclear pore complex and of distinct pore complex components. *J. Cell Biol.* **110:**883–894

Ruknudin, A., Sachs, F., Bustamante, J.O. 1993. Stretch-activated channels of chick cardiac myocytes. *Am. J. Physiol.* **264:**H960–H972

Sakmann, B., Neher, E. 1983. Single-Channel Recording. Plenum, New York

Simon, S.M., Blobel, G. 1991. A protein-conducting channel in the endoplasmic reticulum. *Cell* **65:**371–380

Simon, S.M., Blobel, G. 1992. Signal peptides open protein-conducting channels in *E. coli*. *Cell* **69:**677–684

Tabares, L., Mazzanti, M., Clapham, D.E. 1991. Chloride channels in the nuclear membrane. *J. Membrane Biol.* **123:**49–54

Takamatsu, T., Wier, W.G. 1990. High temporal resolution video imaging of intracellular calcium. *Cell Calcium* **11:**111–120

Veenstra, R.D. 1990. Voltage-dependent gating of gap junction channels in embryonic chick ventricular cell pairs. *Am. J. Physiol.* **258:**C662–C672

Waybill, M.M., Yelamarty, R.V., Zhang, Y., Scaduto, Jr., R.C., LaNoue, K.F., Hsu, C.-J., Smith, B.C., Tilloston, D.L., Yu, F.T.S., Cheung, J.Y. 1991. Nuclear calcium transients in cultured rat hepatocytes. *Am. J. Physiol.* **261:**E49–E57

Williams, D.A., Fogarty, K.E., Tsien, R.Y., Fay, F.S. 1985. Calcium gradients in single smooth muscle cells revealed by the digital imaging microscope using Fura-2. *Nature* **318:**558–561